Chinese Chemical Letters 35 (2024) 109130

Contents lists available at ScienceDirect

Chinese Chemical Letters

journal homepage: www.elsevier.com/locate/cclet

Selective removal of Cr(VI) using polyvinylpyrrolidone and polyacrylamide co-modified MoS_2 composites by adsorption combined with reduction

Shuqi Yu[a], Yu Yang[a,*], Keisuke Kuroda[b], Jian Pu[c], Rui Guo[d,*], Li-An Hou[a]

[a] State Key Laboratory of Water Environment Simulation, School of Environment, Beijing Normal University, Beijing 100875, China
[b] Department of Environmental and Civil Engineering, Toyama Prefectural University, Imizu, Toyama 939-0398, Japan
[c] Institute for the Advanced Study of Sustainability, United Nations University, Jingumae 5-53-70, Shibuya-ku, Tokyo 150-8925, Japan
[d] Technical Centre for Soil, Agriculture and Rural Ecology and Environment, Ministry of Ecology and Environment, Beijing 100012, China

ARTICLE INFO

Article history:
Received 21 May 2023
Revised 22 August 2023
Accepted 19 September 2023
Available online 1 October 2023

Keywords:
Polyvinylpyrrolidone
Polyacrylamide
MoS_2
Cr(VI) removal
Adsorbent
Reduction

ABSTRACT

Cr(VI), one of the most hazardous metal pollutants, poses significant threats to the environment and human health. Herein, a novel MoS_2 composite (MoS_2/PVP/PAM) modified by polyvinylpyrrolidone (PVP) and polyacrylamide (PAM) was synthesized to enhance the removal of Cr(VI). Characterization analysis including SEM, XRD, FTIR, and XPS indicated that PVP and PAM could increase the interlayer spacing and the dispersibility of MoS_2, and introduce pyrrolic N and amino functional groups. The batch experiments showed that MoS_2/PVP/PAM represented excellent Cr(VI) removal performance over a wide pH range, and exhibited a significantly higher maximum Cr(VI) adsorption capacity (274.73 mg/g, at pH 3.0, and 298 K) than pure MoS_2. The adsorption of Cr(VI) followed Langmuir and *pseudo*-second-order kinetic model, which was a homogeneous monolayer chemisorption process. MoS_2/PVP/PAM showed stable removal of Cr(VI) in the presence of humic acid (HA), interfering cations and anions at different concentrations. Moreover, it had excellent selectivity for Cr(VI) (K_d value of 1.69×10^7 mL/g) when coexisting with a variety of competing ions. Multiple characterization revealed that Cr(VI) was reduced to low toxicity Cr(III) by Mo^{4+} and S^{2-}, and then chelated on the surface of the adsorbent by pyrrolic N. This research expanded the design concept for MoS_2 composites by demonstrating the potential of MoS_2/PVP/PAM as a promising material for selective elimination of Cr(VI) in water.

© 2024 Published by Elsevier B.V. on behalf of Chinese Chemical Society and Institute of Materia Medica, Chinese Academy of Medical Sciences.

In light of the rapid development of urbanization and industrialization, the excessive emission of various harmful heavy metals (including Pb, Cu, Hg, Cd and Cr) into the environment has become a global concern [1]. Among them, chromium (Cr) is one of the most typical pollutants, which is widely found in industrial wastewater generated by metallurgy, electroplating, tanning, textile, and other industries [2]. Cr(III) and Cr(VI) are the two most prevalent chromium forms in the environment. Among them, Cr(III) is one of the essential trace elements for human health, as it can help to regulate blood sugar and lower cholesterol levels [3]. Nevertheless, Cr(VI) is one of the three metals that are recognized internationally as being carcinogenic, because of its harmful effects on human health such as skin, kidney and liver diseases, as well as the elevated risk of genetic damage (*e.g.,* cancer, fetal malformations) [4,5]. Cr(VI) is listed as the first type of pollutant in China's industrial wastewater discharge standards [6]. Therefore, it has become a critical environmental issue to effectively remove Cr(VI) from wastewater.

To date, there are a number of technologies developed for Cr(VI) removal from water, such as membrane filtration [7], chemical precipitation [8], photocatalysis [9], ion exchange [10], electrochemistry [11], and adsorption [12]. Due to the low operating costs, ease of operation, and high efficiency, the adsorption method gained extensive interest [13]. Conventional adsorbents such as metal oxides [14], zeolite [15], clay [16], and activated carbon [17] have been used extensively for Cr(VI) adsorption. However, they generally have low selectivity and adsorption capacity. It is therefore crucial to develop adsorbents with excellent selectivity and adsorption capacity.

As one of the typical representatives of transition metal sulfide, the two-dimensional molybdenum disulfide (MoS_2) has shown great promise in numerous environmental applications [18,19]. MoS_2 has been applied to remove heavy metal ions and organic

* Corresponding authors.
E-mail addresses: yangyu@bnu.edu.cn (Y. Yang), guorui3030@163.com (R. Guo).

https://doi.org/10.1016/j.cclet.2023.109130
1001-8417/© 2024 Published by Elsevier B.V. on behalf of Chinese Chemical Society and Institute of Materia Medica, Chinese Academy of Medical Sciences.

contaminants due to its abundant sulfur active sites, large specific surface area, and remarkable chemical stability [20,21]. The inherent S atom on the surface of MoS_2, as a soft base, can effectively remove heavy metal ions such as Pb(II), Hg(II), and Cu(II) in water through the Lewis soft acid-soft base interaction. Furthermore, MoS_2 can potentially transform Cr(VI) to low toxicity Cr(III) in solution under protonation conditions due to its significant protonation ability and strong electron transfer potential [22]. However, it remains a great challenge to apply MoS_2 for removing Cr(VI) from water. MoS_2 tends to agglomerate and interlayer stacking because of the high surface energy associated with the interlayer van der Waals forces, which reduce the specific surface area and active sites for removing Cr(VI) [23,24]. In addition, the removal efficiency of MoS_2 for Cr(VI) is not satisfactory due to the lack of active functional groups to adsorb Cr(VI).

In recent years, the polyvinylpyrrolidone (PVP) and polyacrylamide (PAM) as polymer materials have drawn increased attention due to their low cost, excellent environmental stabilization, outstanding capacitance performance, and prominent biological compatibility [22]. The dispersibility and stability of MoS_2 are improved by coating with high molecular polymer [25]. During the hydrothermal synthesis process, PVP, a typical nonionic surfactant, may preferentially adsorb on the specific crystal planes of materials, preventing restacking and improving the structural stability of MoS_2 layers [26–28]. PAM is a cationic surfactant with large molecular weight and hydrophilic groups that can improve the dispersibility of materials in highly polar solvents [29]. In addition, considering that PVP and PAM contain rich amide and amino groups, they can combine with anions such as CrO_4^{2-} and $HCrO_4^-$, thus providing abundant adsorption sites to effectively capture Cr(VI) ions from the mixture. By adding PVP and PAM to improve the dispersibility of MoS_2, increasing the exposure of S atoms, and introducing amide and amino functional groups, the removal ability of MoS_2 to Cr(VI) will be effectively improved.

Here, Cr(VI) was removed from wastewater using MoS_2 composites with PVP and PAM co-modifications (MoS_2/PVP/PAM), which were synthesized using an efficient hydrothermal process. The existence of PVP and PAM can prevent MoS_2 from agglomerating and promote its dispersity while providing more binding sites for Cr(VI). Batch experiments were used to thoroughly investigate the effects of several environmental variables on Cr(VI) elimination, including pH, contact time, temperature, coexisting ions, and humic acid. Besides, X-ray photoelectron spectroscopy (XPS) was utilized to probe the Cr(VI) reaction mechanism. Overall, this investigation provided new insight into removing Cr(VI), and also broadened the modification methods of MoS_2 composites.

The preparation process for MoS_2/PVP/PAM was described in detail in Supporting information. SEM and TEM characterization were performed to observe the material morphology. As depicted in Fig. 1a, MoS_2 was a corrugated nanoflower structure formed from thousands of nanosheets and was in an agglomerated state. After doping PVP and PAM (Figs. 1b-d), MoS_2/PVP, MoS_2/PAM, and MoS_2/PVP/PAM had similar morphologies, and were randomly stacked by sheet-like structures. As shown in Figs. 1e-h, the dispersibility of MoS_2/PVP/PAM was significantly improved, and the edges became thinner and more transparent, indicating that MoS_2/PVP/PAM had an ultrathin nanosheet morphology. The results suggested that PVP and PAM had a synergistic effect on improving the dispersion of MoS_2. The HRTEM images (Figs. 1i-l) revealed clear MoS_2/PVP/PAM lattice fringes with adjacent lattice spacings of 7.2 and 2.7 Å, which corresponded to the *d*-spacing of (002) and (100) lattice planes for MoS_2 [30]. Besides, the (002) spacing of the MoS_2/PVP, MoS_2/PAM, and MoS_2/PVP/PAM increased to 7.2, 6.9, and 7.2 Å, respectively, which was greater than that of pure MoS_2 (6.5 Å), possibly as a result of PVP and PAM adsorption into MoS_2 layers during the hydrothermal synthesis process, and PVP had a more significant impact on increasing the layer spacing of MoS_2 compared with PAM. The expanded interlayer spacing can not only provide a channel for ion diffusion and transport, but also offer a large number of active sites, potentially enhancing Cr(VI) removal. Furthermore, the elemental mapping images (Fig. 1m) revealed that the elements C, N, S, Mo, and O were homogeneously distributed across the MoS_2/PVP/PAM surface.

Fig. S1a (Supporting information) showed the XRD patterns of various materials. The obvious characteristic peaks at $2\theta = 13.44°$, 32.17°, 35.18°, and 57.51° were attributed to the MoS_2 lattice planes (002), (100), (102), and (110), respectively [3]. After modification, the characteristic peak position of the (002) lattice plane was moved from 13.44° to 12.25°, which was attributed to the intercalation of PVP and PAM into MoS_2 layers and led to lattice expansion [31]. It was in consistency with the increased interlayer spacing in HRTEM pictures that the interlayer spacing of MoS_2/PVP/PAM (7.22 Å) was greater than that of pure MoS_2 (6.58 Å), exposing previously unavailable sulfur atoms.

The functional groups of prepared composites were confirmed by FTIR spectroscopy. According to Fig. S1b (Supporting information), the stretching vibration of Mo-S was responsible for an absorption peak in the spectra of MoS_2 at 615.19 cm^{-1} [30]. The peaks at 899.97, 1019.07, 1104.18, and 1397.48 cm^{-1} were associated with the Mo–O, S–O, C–O–C, and C–OH vibrations [32]. The peaks at 1596.04 and 3413.15 cm^{-1} were responsible for the bending and stretching vibrations of O–H in adsorbed water molecules [31]. As for MoS_2/PVP/PAM composites, the bands at 1225.38, 1484.94, and 1619.42 cm^{-1} corresponded to the stretching vibration of C–N, C–C ring, and C=O from the amide functional group in PVP and PAM, respectively [33,34]. The above analysis confirmed that PVP and PAM with abundant amide and amino groups were successfully doped into the composites. The introduction of amide and amino functional groups will help to further improve the Cr(VI) elimination capacity of MoS_2/PVP/PAM.

Furthermore, according to BET analysis, the total volume of pores and BET specific surface area of MoS_2, MoS_2/PVP, MoS_2/PAM, and MoS_2/PVP/PAM were 0.075, 0.080, 0.057, 0.086 cm^3/g, and 23.14, 34.04, 21.70, 35.41 m^2/g, respectively (Figs. S1c and d in Supporting information). In comparison to MoS_2 and other modified materials, MoS_2/PVP/PAM had a greater pore volume and specific surface area, showing that PVP and PAM had a synergistic effect on preventing the aggregation of MoS_2 in the aqueous solution. Compared with MoS_2 (26.24 nm), the pore diameter of MoS_2/PVP/PAM (38.34 nm) increased (Table S1 in Supporting information), which was beneficial to improve diffusion and accelerate the Cr(VI) adsorption. Therefore, this method effectively improved the dispersity of MoS_2/PVP/PAM, and more potential active sites for Cr(VI) adsorption were exposed, which was favorable for heavy metal ions removal.

In general, solution pH had a significant impact on adsorption performance. As depicted in Fig. S2a (Supporting information), the removal efficiency improved gradually as the pH decreased, suggesting that the acidic condition was conductive to Cr(VI) removal. MoS_2/PVP/PAM composites had an evident improvement in adsorption capacity from 95.44 mg/g (pH 11.0) to 212.28 mg/g (pH 3.0). As shown in Fig. S2b (Supporting information), $HCrO_4^-$ and $Cr_2O_7^{2-}$ were the predominant Cr(VI) species in the pH 2.0–6.0 range, while CrO_4^{2-} was the dominant specie at pH > 6.0, and H_2CrO_4 was negligible in the range of pH 2.0–12.0 [35]. $HCrO_4^-$ required less adsorption free energy and utilized fewer adsorption sites than CrO_4^{2-}, so it was more readily adsorbed on materials. $HCrO_4^-$ and $Cr_2O_7^{2-}$, which are oxidizing ions, can react with the reducing functional group (S-Mo-S) on the surface of MoS_2/PVP/PAM under protonation conditions at low pH [13]. Nevertheless, because of the deprotonation on the MoS_2/PVP/PAM surface, the negative charge density of the

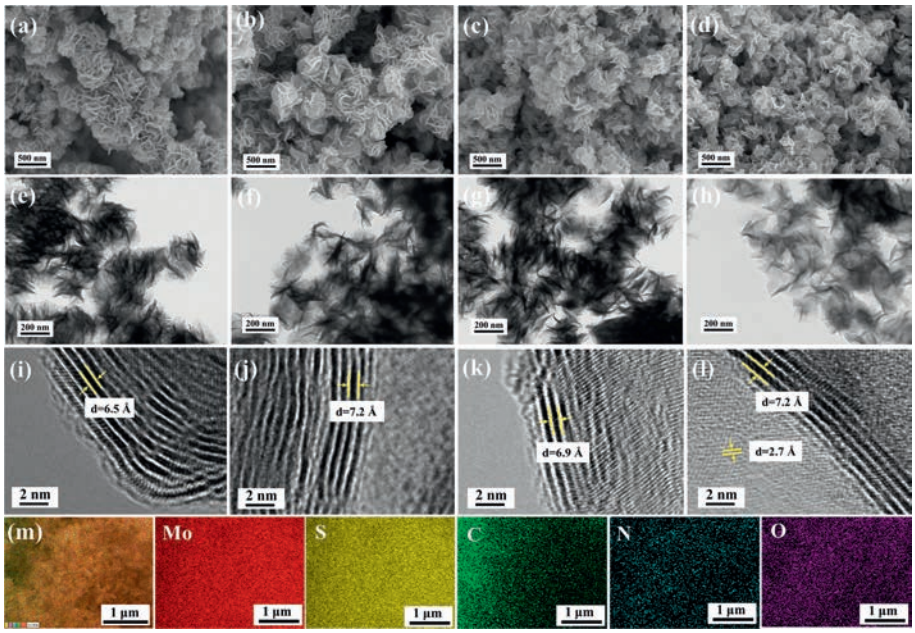

Fig. 1. SEM, TEM, and HRTEM images. (a-d) SEM images for MoS_2, MoS_2/PVP, MoS_2/PAM, and MoS_2/PVP/PAM, respectively. (e-h) TEM images for MoS_2, MoS_2/PVP, MoS_2/PAM, and MoS_2/PVP/PAM, respectively. (i-l) HRTEM images for MoS_2, MoS_2/PVP, MoS_2/PAM, and MoS_2/PVP/PAM, respectively. (m) Elemental mapping images of MoS_2/PVP/PAM.

adsorbent surface grew as the solution pH increased, which significantly increased the electrostatic repulsion force between adsorbents and CrO_4^{2-}, and caused the removal efficiency to decline at high pH. Furthermore, the hydroxyl group and Cr(VI) competed for binding sites, which also led to the decline of removal performance under alkaline conditions. Thus, the adsorbent surface characteristics and Cr(VI) chemical species, which were affected by the change of solution pH change, lead to a significant decrease in Cr(VI) elimination efficiency as pH increased. Considering that, many chromium-contained wastewaters, such as electroplating wastewater and metal pickling wastewater, were acidic [23]. Therefore, the ideal pH for subsequent experiments was pH 3.0.

Although the four composites showed high removal efficiency in acidic solution, the Cr(VI) removal advantage of MoS_2/PVP/PAM over the others gradually became prominent as pH increased. At pH 11.0, the adsorption capacity of MoS_2/PVP/PAM was 2.30, 1.46, and 1.41 times higher than that of MoS_2, MoS_2/PVP, and MoS_2/PAM, respectively. The zeta potentials of all prepared materials were negative at all pH values (Fig. S3 in Supporting information). The removal effect of materials was related to various factors, such as specific surface area and surface functional groups. After simultaneous modification with PVP and PAM, the variety of functional groups on the surface of the materials was abundant, resulting in improved removal performance at different pH. The results showed that MoS_2/PVP/PAM maintained a high removal rate in acid and alkali solutions, and had great potential in practical application.

To examine the removal capacities of the prepared composites, the Langmuir and Freundlich models were devoted to investigate the interaction between Cr(VI) and adsorbents. Eqs. S2 and S3 (Supporting information) describe the equations of the Langmuir and Freundlich models, respectively. Figs. 2a and b displayed the fitting diagrams of Langmuir and Freundlich adsorption isotherm of Cr(VI) from different materials, and Table S2 (Supporting information) provided the relevant parameters. For the four adsorptions, the Langmuir model was superior to the Freundlich model for Cr(VI) adsorption, demonstrating that the Cr(VI) elimination process was monolayer adsorption on composites. The maximum adsorption capacity of MoS_2, MoS_2/PVP, MoS_2/PAM, and MoS_2/PVP/PAM at 298 K for Cr(VI) reached 180.18, 236.97, 203.67, and 274.73 mg/g, respectively. It could be speculated that both the pyrrolic N in PVP and amine in PAM promoted the elimination ability of Cr(VI) from MoS_2/PVP/PAM, which was verified by XPS spectra. In addition, the $1/n$ value was between 0 and 0.5, suggesting that the adsorption process was favorable for chemisorption [31].

Another important parameter (R_L) is also applied to determine whether the adsorption process is beneficial or unfavorable, which is calculated using Eq. S4 (Supporting information). The R_L values of Cr(VI) on MoS_2/PVP/PAM ranged between 0 and 1 (R_L: 0.023–0.108, meaning favorable), further confirming that the removal of Cr(VI) was favorable at different temperatures. Additionally, the maximum Cr(VI) adsorption capacity on MoS_2/PVP/PAM increased from 274.73 at 298 K to 327.87 mg/g at 318 K (Figs. S4a and b, and Table S3 in Supporting information), showing that the Cr(VI) elimination was improved by the elevated temperature. Table S4 (Supporting information) summarized the maximum adsorption capabilities of MoS_2-based modified composites for Cr(VI). MoS_2/PVP/PAM had a greater ability to eliminate Cr(VI) than the other MoS_2-based materials, yet its synthesis process was relatively simple. Therefore, it could be concluded that MoS_2/PVP/PAM had a great prospect in the purification of chromium-containing wastewater.

The thermodynamic parameters involved in Cr(VI) adsorption on MoS_2/PVP/PAM were calculated according to Eqs. S5–S7 (Supporting information). Table S5 (Supporting information) showed the calculated thermodynamic parameters. The ΔG^0 was between −5.21∼−6.47 KJ/mol and decreased as the temperature rose, indicating that a temperature increase was beneficial to the spontaneous enhancement of the reaction (Fig. S4d in Supporting information). The value of ΔH^0 and ΔS^0 was positive, further revealing that the reaction process was endothermic, and the randomization was enhanced during adsorption.

To gain a better understanding of the removal process, the experimental data were simulated using *pseudo*-first-order and *pseudo*-second-order adsorption kinetic models (Eqs. S8 and S9 in Supporting information). As presented in Fig. S5a (Supporting information), the adsorption efficiency grew significantly during the

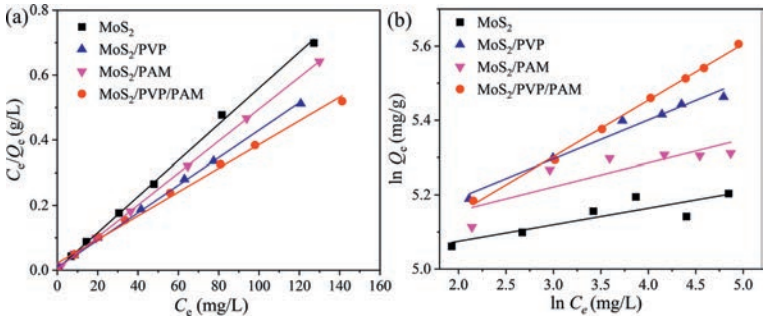

Fig. 2. The linear Cr(VI) adsorption isotherms of (a) Langmuir and (b) Freundlich by MoS_2, MoS_2/PVP, MoS_2/PAM, and MoS_2/PVP/PAM ($C_0 = 20–150$ mg/L, pH 3.0, $m/V = 0.4$ g/L).

first 2 h of contact, and remained at a high level as adsorption time increased until equilibrium was attained. In the meantime, the equilibrium Cr(VI) adsorption capacity of MoS_2/PVP/PAM was better than that of MoS_2, demonstrating that MoS_2/PVP/PAM displayed superior Cr(VI) removal capacity. As demonstrated in Figs. S5b and c and Table S6 (Supporting information), the *pseudo*-second-order kinetic model had a superior fitting effect to the *pseudo*-first-order kinetic model, indicating a primarily chemical adsorption in the reaction.

Weber and Morris interparticle diffusion model (Eq. S10 in Supporting information) was used to further investigate the kinetic data. The relevant parameters of MoS_2 and MoS_2/PVP/PAM were presented in Table S7 (Supporting information). Fig. S5d (Supporting information) showed three separate linear zones, demonstrating that the Cr(VI) elimination involved a multi-step reaction [3]. In the first stage (up to 1 h), the slope (k_1) and removal rate were the highest, which was consistent with Cr(VI) diffusing from the solution to the adsorbent outer surface under the effect of boundary membrane diffusion. The removal efficiency increasingly slowed down and the diffusional resistance improved in the second stage (2–10 h), indicating that this stage was mainly determined by intra-particle diffusion, *i.e.*, Cr(VI) entered the intra-particle and pores from the exterior surface of composites. After that, because of the reduction of adsorbent binding sites, the internal diffusion rate of the particles gradually declined, and finally reached the equilibrium stage. Furthermore, the fitted curve did not go through the origin, indicating that membrane diffusion, in addition to intraparticle diffusion, was also the rate-limiting step in controlling Cr(VI) elimination [36]. It was clear that the rate constant and the removal efficiency of MoS_2/PVP/PAM were greater than those of MoS_2 at each stage, suggesting that MoS_2/PVP/PAM had more surface active sites and more easily reacted with Cr(VI).

The common ions and Cr(VI) in natural water and industrial wastewater may have plenty of competition for adsorption sites, which could affect the removal process of Cr(VI). Therefore, the influence of common anions and cations at 10 mmol/L and 30 mmol/L concentrations on the elimination of Cr(VI) by MoS_2/PVP/PAM was researched (Fig. 3a). When introducing the different types of ions in the adsorption system, no significant fluctuations were observed in the presence of anions (*e.g.*, NO_3^- and Cl^-) and cations (*e.g.*, Na^+, Mg^{2+}, K^+ and Ca^{2+}), and the adsorption capacity remained unchanged. Because Cr(VI) existed in the form of an anion ($HCrO_4^-$), while Na^+, K^+, Ca^{2+}, and Mg^{2+} existed as a cation, which did not compete with the adsorption sites of Cr(VI) [37]. In addition, the redox potential of Na^+ (−2.71 V), K^+ (−2.97 V), Mg^{2+} (−2.37 V), and Ca^{2+} (−2.87 V) is smaller than Cr^{6+} (1.35 V) and did not affect the reduction of Cr(VI) [38]. Negatively charged Cl^- and NO_3^- were expected to compete with Cr(VI) for adsorption sites on the material surface. However, since Cl^- and NO_3^- were low-affinity ligands, their interactions with adsorption sites are weak in solution, so their competitive effects in the Cr(VI) adsorption process can be neglected [39]. Interestingly, SO_4^{2-} and CO_3^{2-} enhanced the Cr(VI) elimination by MoS_2/PVP/PAM. As presented in Fig. S6 (Supporting information), with the addition of SO_4^{2-} and CO_3^{2-}, the content of Cr(VI) was less detected, while the proportion of Cr(III) remarkably increased. This phenomenon suggested that SO_4^{2-} and CO_3^{2-} could facilitate the Cr transition on the adsorbent surface from Cr(VI) to Cr(III), and Cr(III) entered the solution, thus releasing more binding sites for Cr(VI) adsorption [40]. On the other hand, SO_4^{2-} and CO_3^{2-} can remove oxides from the surface of the materials, thereby destroying the passivation film and increasing the active sites of MoS_2/PVP/PAM [38].

Humic acid (HA) is the most common organic compound in the natural water environment [41]. The influence of different HA concentrations on the elimination of Cr(VI) was depicted in Fig. 3b. There was no discernible difference in the removal of Cr(VI) under various concentrations of HA, revealing that HA had little competition for Cr(VI) adsorption sites, due to the weak binding ability between HA and the active site on the adsorbents [42]. Overall, these results indicated that MoS_2/PVP/PAM exhibited stable Cr(VI) removal performance under the coexistence of ions or organics, and had promising application prospects in practical wastewater treatment.

Considering the complexity of real water, the selectivity of MoS_2/PVP/PAM for Cr(VI) removal was studied in a mixed heavy metal solution system containing Ni(II), Zn(II), Cd(II), Co(II), and Cu(II) (Fig. 3c). The adsorption capacities of MoS_2/PVP/PAM was 245.49 mg/g for Cr(VI) and 95.40 mg/g for Cu(II), and less than 10 mg/g for Ni(II), Co(II), Zn(II) and Cd(II), respectively. S atoms in MoS_2 were able to adsorb Cu(II) through the Lewis soft-base interaction, with the adsorption capacity second only to Cr (VI). The distribution coefficient (K_d) (Eq. S11 in Supporting information) was used to describe the adsorption selectivity of Cr(VI) and five competing ions on MoS_2/PVP/PAM. As shown in Fig. 3d, MoS_2/PVP/PAM exhibited an ultra-high K_d value of 1.69×10^7 mL/g, which was much higher than other competing metal ions. It is generally believed that adsorbents with a K_d value greater than 1.0×10^5 mL/g had great affinity and selectivity [43], indicating that MoS_2/PVP/PAM exhibited preferential binding and enormous selectively for Cr(VI). The reduction of Cr(VI) by MoS_2/PVP/PAM was one of the important reasons for its high selectivity. In conclusion, the removal performance of MoS_2/PVP/PAM for Cr(VI) was much greater than those of coexisting ions in a mixed heavy metal system.

The reusability was a crucial index to evaluate the actual applicability potential of adsorbents. As a portion of adsorbed Cr(VI) was reduced to Cr(III), to release Cr(VI) and Cr(III) adsorbed on composites, the MoS_2/PVP/PAM was successively treated with 0.2 mol/L NaOH and HCl for the subsequent adsorption cycle experiments. The adsorption capacity gradually dropped as the cycle

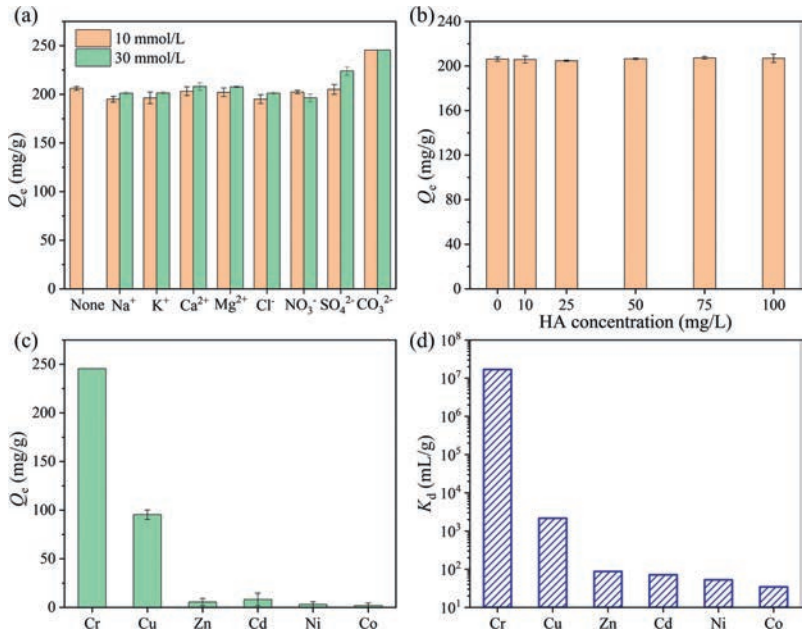

Fig. 3. Impact of (a) coexisting ions and (b) humic acid on Cr(VI) removal by MoS_2/PVP/PAM. (c) Adsorption capacity of MoS_2/PVP/PAM for Cr(VI) and competitive ions in mixed heavy metal system. (d) Distribution coefficient (K_d) of Cr(VI) and competitive ions ($C_0 = 100$ mg/L, $C_{ion} = 1.92$ mmol/L, pH 3.0, $m/V = 0.4$ g/L).

number increased, and then declined to 71.95% in the fourth cycle (Fig. S7a in Supporting information). The decreased Cr(VI) adsorption might be caused by undesorbed Cr(III) occupying binding active sites, and by the depletion of Mo^{4+} and S^{2-} for Cr(VI) reduction (the generation of Mo^{6+} and SO_4^{2-} was confirmed in XPS spectra). But the adsorption capacity was still above 150 mg/g in the fourth cycle, indicating that the MoS_2/PVP/PAM had good recyclability for Cr(VI) adsorption. Additionally, the leaching concentration of Mo ions in each cycle experiment was investigated to assess the stability of MoS_2/PVP/PAM and to check the release of Mo ions in the adsorbents. As shown in Fig. S7b (Supporting information), as the cycle number increased, the Mo ion concentration leached from MoS_2/PVP/PAM gradually decreased, and always remained at a low level. The reason for the slight Mo leaching was that a portion of Mo ions was present in MoS_2/PVP/PAM as Mo^{6+}, and some Mo was oxidized to Mo^{6+} during the reduction of Cr(VI). Since Mo^{6+} ions were easily released into the solution, the amount of Mo released gradually decreases with the number of cycles increasing [3], showing that MoS_2/PVP/PAM had satisfying cycle stability in Cr(VI) elimination.

To explore the adsorption mechanism between Cr(VI) and adsorbents, the XPS spectra of MoS_2/PVP/PAM before and after adsorption were examined (Fig. 4). The peaks of S 2p, Mo 3d, C 1s, N 1s, and O 1s could be observed at 161.58, 228.61, 284.87, 394.62, and 531.43 eV, respectively (Fig. 4a). After the reaction with Cr(VI), a significant peak was detected at 577.27 eV in comparison to the pristine composites, demonstrating that MoS_2/PVP/PAM successfully captured Cr(VI). The peak of Cr 2p was further separated into four peaks corresponding to Cr(III) $2p_{3/2}$ (576.41 eV), Cr(VI) $2p_{3/2}$ (577.83 eV), Cr(III) $2p_{1/2}$ (585.95 eV), and Cr(VI) $2p_{1/2}$ (587.66 eV), as shown in Fig. 4b. This suggests that Cr(VI) and Cr(III) coexisted on the MoS_2/PVP/PAM surface. The presence of Cr(III) implied that in addition to the adsorption reaction, a redox reaction also occurred [44]. According to the high deconvolution data listed in Table S8 (Supporting information), the peak area ratio of Cr(III) (60.10%) and Cr(VI) (39.90%) confirmed that most Cr(VI) was converted to Cr(III).

According to Figs. 4c and d, and Table S8 (Supporting information), the surface binding energies of Mo $3d_{3/2}$, Mo $3d_{5/2}$, S $2p_{3/2}$, and S $2p_{1/2}$ shifted slightly after the reaction with Cr(VI), which showed that Mo and S participated in the process of Cr(VI) elimination [45,46]. MoS_2/PVP/PAM was able to reduce Cr(VI), because compared with the $HCrO_4^-/Cr^{3+}$ pair (approximately 1.35 V), the redox potential of the MoO_4^{2-} and SO_4^{2-}/MoS_2 pair (approximately 0.429 V) was significantly lower [30,47]. According to the adsorption spectra of Mo 3d and S 2p, the more obvious peaks of Mo^{6+} and SO_4^{2-} further confirmed the redox reaction. After the reaction, the peak area of SO_4^{2-} in S 2p increased from 6.42% to 39.12%, and the peak area of Mo^{6+} in Mo 3d increased from 4.45% to 20.32% (Table S8), indicating that S^{2-} was more important than Mo^{4+} in Cr(VI) reduction. In addition, the O 1s peak signal intensity in the XPS full-spectrum scan was significantly enhanced after adsorption, which indicated the soluble molybdate and sulfate ions were generated after Cr(VI) removal. Hence, the following formula was used to describe the chemical reaction between adsorbents and Cr(VI) [45]:

$$6HCrO_4^- + MoS_2 + 6H^+ \rightarrow 6Cr^{3+} + MoO_4^{2-} + 2SO_4^{2-} + 12OH^-$$

The chemical equation predicted that while the reaction continued, the alkalinity of the solution gradually increased. It was found that the solution pH increased from 3.01 to 4.11, by monitoring the solution pH during the reaction, which demonstrated that OH^- was released into the solution during the reaction.

Fig. 4e showed the high-resolution spectra of O 1s, where the peaks at 530.62 eV and 532.10 eV corresponded to C–C=O and N–C=O, respectively [31]. The binding energy of C–C=O changed to 530.72 eV, and the peak area increased from 63.57% to 74.16%. Meanwhile, the peak of N–C=O shifted to 532.35 eV, and the peak area decreased from 36.43% to 25.84%, suggesting that the oxygen-containing groups of MoS_2/PVP/PAM synergistically promoted the coordination with Cr(VI) ions [46]. Similarly, Fig. 4f illustrated that the two peaks of N 1s spectra were separated into 398.61 eV and 400.19 eV, which corresponded to pyrrolic N and amine (-NH_2), respectively [48,49]. After the adsorption, the binding energy and peak area of amine and pyrrolic N were changed, suggesting that amine and pyrrolic N participated in Cr(VI) removal. Especially, pyrrolic N could reduce Cr(VI) to Cr(III), and subsequently Cr(III) interacted with N to form a complex *via* covalent interaction. Furthermore, a new peak occurred at 403.92 eV, representing the pro-

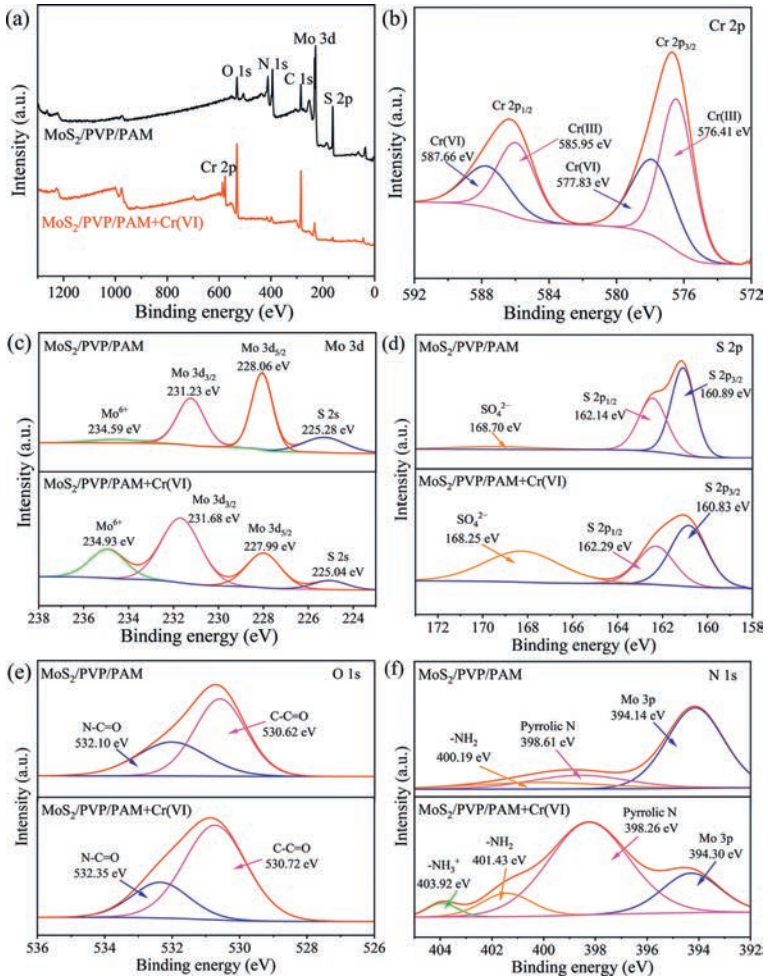

Fig. 4. XPS spectra of MoS_2/PVP/PAM before and after adsorption: (a) Full survey spectra; (b) peaks of Cr 2p; (c) peaks of Mo 3d; (d) peaks of S 2p; (e) peaks of O 1s and (f) peaks of N 1s.

tonated amine group ($-NH_3^+$) [50], which favored the electrostatic attraction with Cr(VI). These findings indicated that pyrrolic N and amine groups in PVP and PAM were crucial to remove Cr(VI).

Besides, according to the change of Cr(III), Cr(VI), and total Cr contents in solution over the reaction time (Fig. S8 in Supporting information), the relation between the Cr(VI) reduction, Cr(VI) adsorption and Cr(III) fixation on MoS_2/PVP/PAM was illustrated. Notably, the total Cr concentration was consistently higher than Cr(VI) due to the Cr(III) production. After adsorption for 5 min, a significant amount of Cr(III) was discovered (12.40 mg/L), and the Cr(III) content remained at 12–16 mg/L for the first 2 h of the reaction, and then steadily fell to 3 mg/L. After the 10 h reaction, the content of Cr(VI) continued to decline slowly as the adsorption time increased, indicating that Cr(VI) was initially reduced to Cr(III), and subsequently the reduced Cr(III) was immobilized on MoS_2/PVP/PAM composites, as predicted by the XPS analysis.

Combined with the analysis of material characterization results, the excellent removal performance of MoS_2/PVP/PAM may be related to the expansion of interlayer spacing, the improvement of dispersion performance, and the introduction of new functional groups. Among them, the introduction of pyrrolidine and amine functional groups in PVP and PAM played a major contribution. As illustrated in Fig. 5, the mechanism of Cr(VI) removal was described as follows: (1) The protonated amine group ($-NH_3^+$) of MoS_2/PVP/PAM adsorbed Cr(VI) *via* electrostatic interaction; (2) The S^{2-} and Mo^{4+} reduced Cr(VI) to Cr(III), and simultaneously

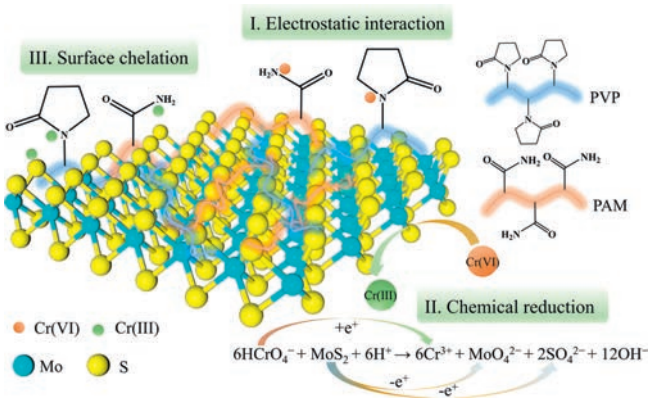

Fig. 5. The elimination mechanism plot of Cr(VI) by MoS_2/PVP/PAM.

were oxidized to SO_4^{2-} and MoO_4^{2-}; (3) Cr(III) was fixed on composites surface *via* forming covalent bonds with pyrrolic N.

Overall, the PVP and PAM co-modified MoS_2 composites (MoS_2/PVP/PAM) were synthesized and used for removing Cr(VI) from water. In batch experiment, PVP and PAM co-modified MoS_2 composites showed an enhanced removal of Cr(VI) (274.73 mg/g), owing to the broadened layer spacing, improved dispersion, and introduced pyrrolic N and amine groups. In addition, PVP and PAM had a synergistic impact on Cr(VI) elimination. More impor-

tantly, the MoS_2/PVP/PAM composites exhibited excellent selectivity under different competing ions and good recyclability. Combined a series of characterization analysis, the removal mechanism of Cr(VI) can be divided into two parts, Cr(VI) was reduced to the low-toxicity Cr(III) by Mo^{4+} and S^{2-}, and then adsorbed on the adsorbent surface by pyrrolic N. This work showed that MoS_2/PVP/PAM composites had a widespread application prospect of Cr(VI) elimination, and provided a new approach for designing MoS_2-based composite materials with enhanced adsorption capacity.

Declaration of competing interest

The authors declare that they have no known competing financial interests or personal relationships that could have appeared to influence the work reported in this paper.

Acknowledgments

This work was supported by the National Natural Science Foundation of China (No. 51920105012), and the National Key Research and Development Program of China (No. 2021YFC3201403).

Supplementary materials

Supplementary material associated with this article can be found, in the online version, at doi:10.1016/j.cclet.2023.109130.

References

[1] Y.D. Zou, X.X. Wang, A. Khan, et al., Environ. Sci. Technol. 50 (2016) 7290–7304.
[2] W.C. Cheng, C.C. Ding, X.X. Wang, et al., Chem. Eng. J. 293 (2016) 311–318.
[3] L. Xiang, C.G. Niu, N. Tang, et al., Chem. Eng. J. 408 (2021) 127281.
[4] D.L. Huang, C.H. Liu, C. Zhang, et al., Bioresour. Technol. 276 (2019) 127–132.
[5] J. Zhang, Y. Ma, W. Zhang, et al., J. Clean. Prod. 365 (2022) 132810.
[6] J.B. Dima, C. Sequeiros, N.E. Zaritzky, Chemosphere 141 (2015) 100–111.
[7] W.H. Yu, Z.Q. Gan, J.R. Wang, et al., J. Membr. Sci. 639 (2021) 119756.
[8] B.H. Xie, C. Shan, Z. Xu, et al., Chem. Eng. J. 308 (2017) 791–797.
[9] N. Luo, C. Chen, D.M. Yang, et al., Appl. Catal. B 299 (2021) 120664.
[10] L.L. Li, X.Q. Feng, R.P. Han, et al., J. Hazard. Mater. 321 (2017) 622–628.
[11] X.H. Li, C.L. Wang, F. Liu, et al., Chem. Eng. J. 404 (2021) 126556.
[12] H.J. Chen, Z.H. Gong, Z.J. Zhuo, et al., Chem. Eng. J. 428 (2022) 132113.
[13] H.J. Chen, Z.B. Zhang, X. Zhong, et al., J. Hazard. Mater. 408 (2021) 124847.
[14] H. Zhang, F. Huang, D.L. Liu, et al., Chin. Chem. Lett. 26 (2015) 1137–1143.
[15] C.D. Zhou, C.Y. Han, X.Z. Min, et al., J. Mol. Liq. 338 (2021) 116619.
[16] H. Najafi, N. Asasian-Kolur, S. Sharifian, J. Mol. Liq. 344 (2021) 117822.
[17] N. Liu, Y.T. Zhang, C. Xu, et al., J. Hazard. Mater. 384 (2020) 121371.
[18] Z. Wang, B. Mi, Environ. Sci. Technol. 51 (2017) 8229–8244.
[19] Y. Zhu, W. Zhao, B. Jing, et al., Chin. Chem. Lett. 34 (2023) 107816.
[20] J. Luo, K. Fu, M. Sun, et al., ACS Appl. Mater. Interfaces 11 (2019) 38789–38797.
[21] C. Liu, Q. Wang, F. Jia, et al., J. Mol. Liq. 292 (2019) 111390.
[22] F.F. Yu, W.K. Song, Z.L. Wu, et al., Sep. Purif. Technol. 294 (2022) 121188.
[23] H. Fan, S. Wang, Z. Qin, et al., ChemistrySelect 5 (2020) 3023–3032.
[24] X.C. Liu, T.L. Wang, G.B. Hu, et al., J. Mater. Sci. Mater. Electron. 29 (2018) 753–761.
[25] X. Wen, C. He, Y.Y. Hai, et al., RSC Adv. 11 (2021) 26391–26402.
[26] Y.L. Jia, Y. Ma, Y.H. Lin, et al., Chem. Phys. 513 (2018) 209–212.
[27] X.F. Wang, Z.R.X. Guan, Y.J. Li, et al., Nanoscale 7 (2015) 637–641.
[28] C.M. Mao, Y. Zhong, H.J. Shang, et al., Chem. Eng. J. 304 (2016) 511–517.
[29] J.F. Shen, J.J. Wu, M. Wang, et al., Adv. Mater. 28 (2016) 8469–8476.
[30] W.T. Cai, D.D. Dionysiou, F.L. Fu, et al., J. Hazard. Mater. 396 (2020) 122728.
[31] J. Wang, X.X. Wang, G.X. Zhao, et al., Chem. Eng. J. 334 (2018) 569–578.
[32] D.Q. Tang, J.H. Li, Z.M. Yang, et al., Chem. Eng. J. 428 (2022) 130954.
[33] P. Pal, J.P. Pandey, G. Sen, Mater. Sci. Eng. B 236 (2018) 32–42.
[34] Y.Y. Yue, S.T. Shen, W.L. Cheng, et al., Colloids Surf. A 636 (2022) 128035.
[35] S. Yang, Q. Li, L. Chen, et al., J. Hazard. Mater. 379 (2019) 120797.
[36] F. Zhao, C.H. Su, W.X. Yang, et al., Appl. Surf. Sci. 527 (2020) 146862.
[37] Y. Li, Y. Gao, Q. Zhang, et al., Sep. Purif. Technol. 258 (2021) 117981.
[38] H. Xu, M.X. Gao, X. Hu, et al., J. Hazard. Mater. 416 (2021) 125924.
[39] Y.L. Xu, J.Y. Chen, R. Chen, et al., Water Res. 160 (2019) 148–157.
[40] X. Tao, X.W. Hu, Z.P. Wen, et al., J. Hazard. Mater. 424 (2022) 127423.
[41] H. Ji, Y. Zhu, J. Duan, et al., Chin. Chem. Lett. 30 (2019) 2163–2168.
[42] Q.Y. Wang, Y. Tian, L.C. Kong, et al., Chem. Eng. J. 425 (2021) 131722.
[43] K.L. Ai, C.P. Ruan, M.X. Shen, et al., Adv. Funct. Mater. 26 (2016) 5542–5549.
[44] H. Ji, Y. Zhu, W. Liu, et al., Colloids Surf. A 561 (2019) 373–380.
[45] Z. Li, R. Fan, Z. Hu, et al., J. Hazard. Mater. 394 (2020) 122525.
[46] P.C. Gu, C.F. Zhao, T. Wen, et al., Chem. Eng. J. 359 (2019) 1563–1572.
[47] Z.Y. Wang, A. Sim, J.J. Urban, et al., Environ. Sci. Technol. 52 (2018) 9741–9748.
[48] C. Sun, G. Song, L. Chen, et al., J. Colloid Interface Sci. 580 (2020) 550–560.
[49] F.Y. Meng, H. Wu, M. Qiao, et al., Langmuir 38 (2022) 1567–1577.
[50] Z.Y. Zhang, T.T. Gao, S.X. Si, et al., Chem. Eng. J. 343 (2018) 207–216.